INSTITUTE OF PHYSICS PUBLISHING SMART MATERIALS AND STRUCTURES
Smart Mater. Struct. **14** (2005) 43–55 doi:10.1088/0964-1726/14/1/005

Mathematical construction of an engineering thermopiezoelastic model for smart composite shells*

Wenbin Yu[1] **and Dewey H Hodges**[2]

[1] Department of Mechanical and Aerospace Engineering, Utah State University, Logan, UT 84322-4130, USA
[2] School of Aerospace Engineering, Georgia Institute of Technology, Atlanta, GA 30332-0150, USA

E-mail: wenbin@engineering.usu.edu

Received 10 May 2004
Published 26 November 2004
Online at stacks.iop.org/SMS/14/43

Abstract
An engineering model for composite piezoelectric shells under mechanical, thermal, and electrical loads has been constructed mathematically using the variational-asymptotic method. This work presents a unique formulation of the nonlinear, three-dimensional, one-way coupled, thermopiezoelasticity problem having the combined merits of both mathematical rigor and engineering simplicity. The variational-asymptotic method is used to rigorously split the three-dimensional problem into two problems: a nonlinear, two-dimensional, shell analysis over the reference surface to obtain the global response, and a linear analysis through the thickness to provide both the generalized shell constitutive model and recovery relations to approximate the original three-dimensional fields. The asymptotically correct electric enthalpy obtained herein is cast into the Reissner–Mindlin form to account for transverse shear deformation including the geometrical refinement due to initial curvatures. Recovery relations have been provided to obtain accurate stress distribution through the thickness. The present model is implemented into the computer program VAPAS. Results for several cases obtained from VAPAS are compared with exact thermopiezoelasticity solutions, classical lamination theory, and first-order shear-deformation theory. An excellent compromise between efficiency and accuracy for analyzing piezoelectric composite shells has been achieved.

1. Introduction

Smart structures have recently received enormous attention [1–3] because of their great potential to meet demanding requirements for structural systems with high strength, high stiffness, light weight, and vibration damping. Among many possible candidates for actuators and sensors, piezoelectrics receive the most attention because they (i) directly relate electrical signals to strain within the material, making them candidates for both actuators and sensors, and (ii) have a wide range of high actuating and sensing frequencies that are suitable for real-time controlling and monitoring. Moreover, in most cases, piezoelectrics are used along with tailored anisotropic materials to maximize the 'intelligence' of the smart structure. While most research has been focused on the behavior of piezoelectric structures under isothermal conditions, an increasing effort has been directed to address the thermopiezomechanical responses [4–6].

Many smart structures have one dimension much smaller than the other two and can be modelled as shells. (Plates are degenerate shells without initial curvature.) The state of the art for analyzing smart shells is limited. Theories are generally derived from three-dimensional (3D) thermopiezoelasticity theory, making use of the fact that the thickness is small in

* Part of this paper was presented at the 45th Structures, Structural Dynamics and Materials Conference, Palm Springs, California, April 19–22, 2004.

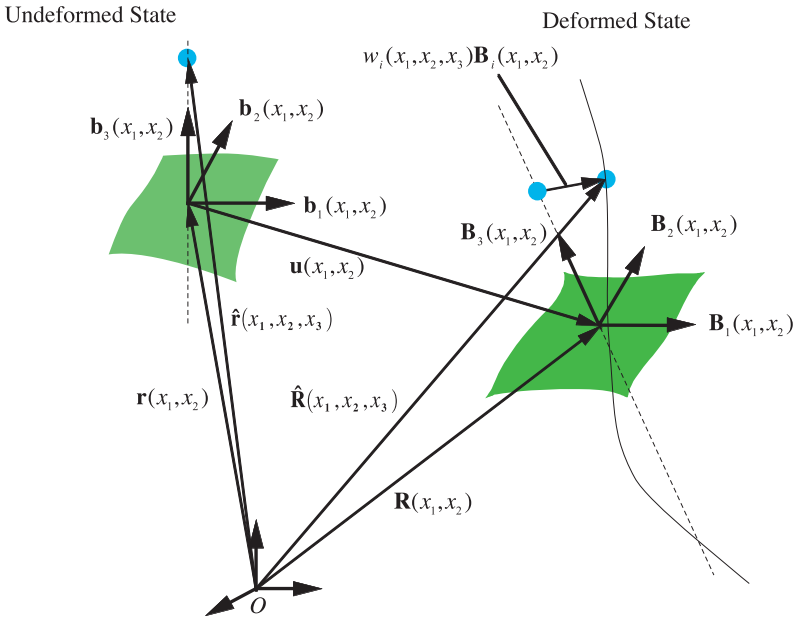

Figure 1. Schematic of shell deformation: initial configuration and deformed configuration.
(This figure is in colour only in the electronic version)

some sense. Most analyses prevailing in the literature are kinematically ad hoc and can be generally classified as classical lamination theories (CLTs) [7], first-order shear-deformation theories (FOSDTs) [8], higher-order theories (HOTs) [6], zig-zag theories [9], and layerwise theories [10]. Layerwise theories can produce reasonable results at the cost of complex models and expensive computation. Although zig-zag theories do indeed yield excellent results for some problems, they have not been proved to be asymptotically correct; only an asymptotically correct theory can be guaranteed to not fail within its derived range of accuracy. All the other ad hoc models are doomed to fail, especially for stress prediction through the thickness of layered shells of moderate thickness. The main reason is that these theories assume the displacements to be C^∞ functions, while in fact displacement functions may have discontinuous derivatives.

From a mathematical point of view, the approximation in the analysis stems from elimination of the thickness coordinate from the independent variables of the governing differential equations. This sort of approximation is inevitable if one wants to take advantage of the smallness of the thickness to simplify the analysis. However, other approximations that are not essential should be avoided. For example, for small-strain analysis of shallow shells, it is reasonable to assume that the thickness, h, is small compared to the wavelength of in-plane deformation, l, and the radius of curvature for the reference surface, R. In contrast, it is not at all rigorous to assume *a priori* some ad hoc displacement field, although that is the way most existing shell theories have been constructed.

Recently a simple and accurate modeling approach for composite plates and shells has been developed, the variational-asymptotic plate and shell (VAPAS) analysis [11–14]. VAPAS starts with an intrinsic formulation of the 3D anisotropic problem in terms of a set of two-dimensional (2D) variables defined for the reference surface and warping of the transverse normal. The intrinsic formulation allows the body to undergo arbitrarily large displacements and global rotations subject only to the restriction that the generalized 2D strains are small. The variational-asymptotic method (VAM) [15] is then adopted to asymptotically reduce the dimensionality of the problem by taking advantage of the small parameters inherent in the problem. As a result, the original nonlinear 3D problem is mathematically split into a linear one-dimensional (1D) through-the-thickness analysis and a nonlinear 2D shell analysis accounting for transverse shear deformation. The through-the-thickness analysis provides a constitutive relation between the generalized 2D strains and stress resultants as well as recovery relations to accurately approximate the 3D displacement, strain, and stress fields in terms of 2D variables calculated in the 2D plate/shell analysis. Although the resulting theory is as simple as a Reissner–Mindlin theory, numerous examples presented in previous works [11–14] demonstrate that the recovered 3D displacement, strain, and stress have excellent accuracy, comparable to that of higher-order, layer-wise theories.

The focus of the present work is to extend the same methodology to model smart composite shells actuated by piezoelectrics so that a simple engineering thermopiezoelastic 2D shell model can be constructed and accurate recovery of the original 3D results can be achieved. The present theory has been implemented into the computer program VAPAS. Several numerical examples for simple problems are provided to validate VAPAS against known 3D exact solutions, to demonstrate the advantages and accuracy of the present model.

2. Three-dimensional formulation

A shell is a 3D body with a relatively small thickness h and a smooth reference surface (see figure 1). The geometry of the reference surface can be described by a set of arbitrary curvilinear coordinates, x_α. (Here and throughout the paper, Greek indices assume values 1 and 2 while Latin indices

assume 1, 2, and 3. Dummy indices are summed over their range except where explicitly indicated.) Without loss of generality, we choose the lines of curvatures to be the curvilinear coordinates to simplify the formulation. To uniquely represent an arbitrary point in a 3D medium, we need another coordinate off the reference surface. We choose it to be the transverse normal, x_3, with $\mathbf{b}_3(x_1, x_2)$ denoting the associated unit vector. Any material point in the undeformed configuration can then be described by its position vector $\hat{\mathbf{r}}$ from a fixed point O as

$$\hat{\mathbf{r}}(x_1, x_2, x_3) = \mathbf{r}(x_1, x_2) + x_3\mathbf{b}_3(x_1, x_2) \tag{1}$$

where $\mathbf{r}$ is the position vector from O to the point located by x_α on the reference surface. If we choose the middle surface of the undeformed shell as the reference surface, we will have

$$\langle \hat{\mathbf{r}}(x_1, x_2, x_3) \rangle = h\mathbf{r}(x_1, x_2) \tag{2}$$

with the angle brackets denoting the definite integral through the thickness of the shell.

The 2D base vectors are defined conventionally as

$$\mathbf{a}_\alpha(x_1, x_2) = \mathbf{r}_{,\alpha} \qquad \text{with } (\,)_{,\alpha} = \frac{\partial(\,)}{\partial\alpha}. \tag{3}$$

From this definition, one obtains the Lamé parameters as

$$A_\alpha(x_1, x_2) = \sqrt{\mathbf{a}_\alpha \cdot \mathbf{a}_\alpha}. \tag{4}$$

Note that the summation convention is not invoked here because α is not a dummy index. This rule will apply in similar situations throughout the rest of the development. The unit vectors along coordinates x_α are

$$\mathbf{b}_\alpha(x_1, x_2) = \frac{\mathbf{a}_\alpha}{A_\alpha}. \tag{5}$$

The unit vectors $\mathbf{b}_i$ form an orthogonal triad. Using equation (3), one can get the 3D covariant base vectors $\mathbf{g}_i = \hat{\mathbf{r}}_{,i}$ for the chosen coordinate system as

$$\mathbf{g}_\alpha = \mathbf{a}_\alpha + x_3\mathbf{b}_{3,\alpha} \qquad \mathbf{g}_3 = \mathbf{b}_3. \tag{6}$$

Following [16], the derivatives of unit vectors $\mathbf{b}_{i,\alpha}$ can be expressed as

$$\mathbf{b}_{i,\alpha} = A_\alpha(-k_{\alpha 2}\mathbf{b}_1 + k_{\alpha 1}\mathbf{b}_2 + k_{\alpha 3}\mathbf{b}_3) \times \mathbf{b}_i \tag{7}$$

where $k_{\alpha\beta}$ refers to the usual out-of-plane curvatures and $k_{12} = k_{21} = 0$ since the coordinates are the lines of curvatures. The geodesic curvatures $k_{\alpha 3}$ can be expressed in terms of the Lamé parameters as

$$k_{13} = -\frac{A_{1,2}}{A_1 A_2} \qquad k_{23} = \frac{A_{2,1}}{A_1 A_2}. \tag{8}$$

Using equation (7), one can obtain the explicit expressions for the 3D covariant and contravariant base vectors:

$$\mathbf{g}_\alpha = A_\alpha(1 + x_3 k_{\alpha\alpha})\mathbf{b}_\alpha \qquad \mathbf{g}^\alpha = \frac{\mathbf{b}_\alpha}{A_\alpha(1 + x_3 k_{\alpha\alpha})} \qquad \mathbf{g}_3 = \mathbf{g}^3 = \mathbf{b}_3. \tag{9}$$

When the shell deforms, the particle that had position vector $\hat{\mathbf{r}}$ in the undeformed state now has position vector $\hat{\mathbf{R}}$ in the deformed shell. The latter can be uniquely determined by the deformation of the 3D body by introducing another triad $\mathbf{B}_i$ for the deformed configuration. Please note that the $\mathbf{B}_i$ vectors are just tools to enable one to express vectors and tensors in their physical components. They are not necessarily tangent to the coordinates of the deformed shell. The relation between $\mathbf{B}_i$ and $\mathbf{b}_i$ can be specified by an arbitrarily large rotation specified in terms of the matrix of direction cosines $C(x_1, x_2)$ so that

$$\mathbf{B}_i = C_{ij}\mathbf{b}_j \qquad C_{ij} = \mathbf{B}_i \cdot \mathbf{b}_j \tag{10}$$

where $\mathbf{B}_i$ is coincident with $\mathbf{b}_i$ when the structure is undeformed. Now the position vector $\hat{\mathbf{R}}$ can be represented as

$$\hat{\mathbf{R}} = \mathbf{R} + x_3\mathbf{B}_3 + w_i(x_1, x_2, x_3)\mathbf{B}_i \tag{11}$$

where w_i is the warping of the normal-line element. These quantities are not assumed, as in most shell theories. Rather, they are treated as unknown 3D functions and their solutions will be obtained later. Equation (11) is six times redundant because of the way warping is introduced. We need to create a one-to-one mapping between $\hat{\mathbf{R}}$ and $(\mathbf{R}, \mathbf{B}_i, w_i)$ by choosing six appropriate constraints. We define $\mathbf{R}$ similarly to equation (2) to be the average position through the thickness, which means the warping functions must satisfy the following three constraints:

$$\langle w_i(x_1, x_2, x_3) \rangle = 0. \tag{12}$$

Two other constraints can be introduced by taking $\mathbf{B}_3$ normal to the reference surface of the deformed shell. It should be understood that this choice has nothing to do with the Kirchhoff–Love hypothesis. In the Kirchhoff–Love assumption, no local deformation of the transverse normal is allowed. However, according to the present scheme, we allow all possible deformation by (a) classifying all deformation beyond that of classical shell theory as warping, (b) assuming that the strain is small, and (c) requiring that the relative rotation of a differential element of the normal line caused by warping is of the order of the strain.

The Jauman–Biot–Cauchy strain tensor for small local rotation is defined in accordance with decomposition of the rotation tensor [17] as

$$\Gamma_{ij} = \tfrac{1}{2}(F_{ij} + F_{ji}) - \delta_{ij} \tag{13}$$

where F_{ij} are the mixed-basis components of the deformation gradient tensor

$$F_{ij} = \mathbf{B}_i \cdot \mathbf{G}_k\mathbf{g}^k \cdot \mathbf{b}_j. \tag{14}$$

Here $\mathbf{G}_k = \hat{\mathbf{R}}_{,k}$ are the covariant basis vectors for the deformed configuration, which can be expressed in terms of the generalized 2D strain measures defined such that [18, 19]

$$\begin{aligned} \mathbf{R}_{,\alpha} &= A_\alpha(\mathbf{B}_\alpha + \varepsilon_{\alpha\beta}\mathbf{B}_\beta) \\ \mathbf{B}_{i,\alpha} &= A_\alpha(-K_{\alpha 2}\mathbf{B}_1 + K_{\alpha 1}\mathbf{B}_2 + K_{\alpha 3}\mathbf{B}_3) \times \mathbf{B}_i \end{aligned} \tag{15}$$

where $\varepsilon_{\alpha\beta}$ are the 2D in-plane strains, the order of which is denoted by ε, and K_{ij} are the curvatures of the deformed surface, the summations of the curvatures of undeformed

geometry k_{ij} and curvatures introduced by the deformation κ_{ij}. Both $\varepsilon_{\alpha\beta}$ and $\kappa_{\alpha\beta}$ are termed as 2D generalized strains. Here one is free to set $\varepsilon_{12} = \varepsilon_{21}$, i.e.

$$\frac{\mathbf{B}_1 \cdot \mathbf{R}_{,2}}{A_2} = \frac{\mathbf{B}_2 \cdot \mathbf{R}_{,1}}{A_1} \tag{16}$$

which serves as the sixth constraint and completely specifies the global rotation of the triad $\mathbf{B}_i$.

With the assumption that the strain is small compared to unity, which has the effect of removing all the terms that are products of the warping and the generalized strains, and with the help of equations (9), (13)–(15), one can obtain the 3D strain field as

$$\begin{aligned}
\Gamma_{11} &= \frac{\varepsilon_{11} + x_3\kappa_{11} + w_{1;1} + w_3 k_{11} - w_2 k_{13}}{1 + x_3 k_{11}} \\
2\Gamma_{12} &= \frac{\varepsilon_{21} + x_3\kappa_{21} + w_{1;2} - w_2 k_{23}}{1 + x_3 k_{22}} \\
&\quad + \frac{\varepsilon_{12} + x_3\kappa_{12} + w_{2;1} + w_1 k_{13}}{1 + x_3 k_{11}} \\
\Gamma_{22} &= \frac{\varepsilon_{22} + x_3\kappa_{22} + w_{2;2} + w_3 k_{22} + w_1 k_{23}}{1 + x_3 k_{22}} \\
2\Gamma_{13} &= w_{1,3} + \frac{w_{3;1} - w_1 k_{11}}{1 + x_3 k_{11}} \\
2\Gamma_{23} &= w_{2,3} + \frac{w_{3;2} - w_2 k_{22}}{1 + x_3 k_{22}} \\
\Gamma_{33} &= w_{3,3}
\end{aligned} \tag{17}$$

where $(\,)_{;\alpha} = (\,)_{,\alpha}/A_\alpha$. Until now, the analysis is as general as a small-strain, geometrically nonlinear theory can be. However, to seek a constitutive model relating the generalized strains and stress resultants, it is inevitable that one has to make some approximations, as mentioned before. It is reasonable to keep the approximations in the constitutive relations since even the original 3D constitutive model is unavoidably approximate.

For most engineering applications, ε is a small parameter in the order of 10^{-5}–10^{-3} and it makes no sense to keep terms in the order of ε in comparison with unity. This fact has already been taken advantage of to derive equation (17). For thin shells, $h/R \sim 10^{-2}$, the components in the order of h/R can be discarded. For shells with moderate thickness ($h/R \sim 10^{-1}$), the geometrical refinement due to h/R is necessary. Numerical examples show that 2D shell models sometimes give satisfactory results down to $h/l \sim 0.5$ [15], which necessitates the construction of shell models that take into account corrections of order h/l and $(h/l)^2$. However, we do not include any correction from $h^2/(Rl)$. This means that the present theory is asymptotically correct for $R > l^2/h$. It is proved in [19] that κ_{21}–κ_{12} is of the order ε/R or $\varepsilon h/l^2$, which only makes a contribution of $\varepsilon(h/R)^2$ or $\varepsilon h^3/(l^2 R)$ to the 3D strain components and is thus outside the range of our approximation. It is worthwhile to emphasize that these approximations are suitable for most engineering shell structures and essentially limit the range of applicability for the shell model. Outside this range deviations from the exact solution can occur.

Having made the above assumptions, one can express the 3D strain field with keeping the terms of order h/R, h/l and $(h/l)^2$ in matrix form as

$$\Gamma = \Gamma_h w + \Gamma_\epsilon \epsilon + \Gamma_{Rh} w + \Gamma_{R\epsilon} \epsilon + \Gamma_{l_\alpha} w_{;\alpha} \tag{18}$$

where

$$\begin{aligned}
\Gamma &= \lfloor\, \Gamma_{11} \quad 2\Gamma_{12} \quad \Gamma_{22} \quad 2\Gamma_{13} \quad 2\Gamma_{23} \quad \Gamma_{33} \,\rfloor^{\mathrm{T}} \\
w &= \lfloor\, w_1 \quad w_2 \quad w_3 \,\rfloor^{\mathrm{T}} \\
\epsilon &= \lfloor\, \varepsilon_{11} \quad 2\varepsilon_{12} \quad \varepsilon_{22} \quad \kappa_{11} \quad \kappa_{12} + \kappa_{21} \quad \kappa_{22} \,\rfloor^{\mathrm{T}}
\end{aligned} \tag{19}$$

and the operators are defined as

$$\Gamma_h = \begin{bmatrix} 0 & 0 & 0 \\ 0 & 0 & 0 \\ 0 & 0 & 0 \\ \frac{\partial}{\partial x_3} & 0 & 0 \\ 0 & \frac{\partial}{\partial x_3} & 0 \\ 0 & 0 & \frac{\partial}{\partial x_3} \end{bmatrix} \qquad \Gamma_{l_1} = \begin{bmatrix} 1 & 0 & 0 \\ 0 & 1 & 0 \\ 0 & 0 & 0 \\ 0 & 0 & 1 \\ 0 & 0 & 0 \\ 0 & 0 & 0 \end{bmatrix}$$

$$\Gamma_{l_2} = \begin{bmatrix} 0 & 0 & 0 \\ 1 & 0 & 0 \\ 0 & 1 & 0 \\ 0 & 0 & 0 \\ 0 & 0 & 1 \\ 0 & 0 & 0 \end{bmatrix} \tag{20}$$

$$\Gamma_\epsilon = \begin{bmatrix} 1 & 0 & 0 & x_3 & 0 & 0 \\ 0 & 1 & 0 & 0 & x_3 & 0 \\ 0 & 0 & 1 & 0 & 0 & x_3 \\ 0 & 0 & 0 & 0 & 0 & 0 \\ 0 & 0 & 0 & 0 & 0 & 0 \\ 0 & 0 & 0 & 0 & 0 & 0 \end{bmatrix}$$

$$\Gamma_{Rh} = \begin{bmatrix} 0 & -k_{13} & k_{11} \\ k_{13} & -k_{23} & 0 \\ k_{23} & 0 & k_{22} \\ -k_{11} & 0 & 0 \\ 0 & -k_{22} & 0 \\ 0 & 0 & 0 \end{bmatrix} \tag{21}$$

$$\Gamma_{R\epsilon} = -x_3 \begin{bmatrix} k_{11} & 0 & 0 & x_3 k_{11} & 0 & 0 \\ 0 & \frac{k_{11}+k_{22}}{2} & 0 & 0 & x_3\frac{k_{11}+k_{22}}{2} & 0 \\ 0 & 0 & k_{22} & 0 & 0 & x_3 k_{22} \\ 0 & 0 & 0 & 0 & 0 & 0 \\ 0 & 0 & 0 & 0 & 0 & 0 \\ 0 & 0 & 0 & 0 & 0 & 0 \end{bmatrix}. \tag{22}$$

To complete the 3D formulation, one needs to provide a constitutive model relating the 3D strains and the stresses. The present interest is to construct a model for smart shells to capture the one-way thermopiezoelastic coupling behavior due to prescribed temperature and electric fields. The changes of temperature and electric fields due to deformation of the shell, and the interactions between temperature and electric fields, are not considered. The 3D constitutive model adopted here is the linear electric enthalpy without the quadratic terms involving temperature and/or electric fields:

$$\begin{aligned}
J &= \int_v \left(\tfrac{1}{2}\Gamma^{\mathrm{T}} D \Gamma - \Gamma^{\mathrm{T}} D\alpha T - \Gamma^{\mathrm{T}} D d\mathcal{E}\right) \mathrm{d}v \\
&= \int_s \left\langle \left(\tfrac{1}{2}\Gamma^{\mathrm{T}} D \Gamma - \Gamma^{\mathrm{T}} D\alpha T - \Gamma^{\mathrm{T}} D d\mathcal{E}\right) \rho \right\rangle \mathrm{d}s
\end{aligned} \tag{23}$$

where v is the volume occupied by the 3D body in the undeformed configuration, s is the surface stretched by the undeformed reference surface and

$$\rho = \frac{\mathbf{g}_1 \times \mathbf{g}_2 \cdot \mathbf{g}_3}{|\mathbf{a}_1 \times \mathbf{a}_2|} = 1 + x_3(k_{11} + k_{22}) + \mathrm{O}\left(\frac{h^2}{R^2}\right). \tag{24}$$

The electric enthalpy per unit area is

$$U = \left\langle \left(\tfrac{1}{2}\Gamma^{\mathrm{T}} D\Gamma - \Gamma^{\mathrm{T}} D\alpha T - \Gamma^{\mathrm{T}} Dd\mathcal{E} \right) \rho \right\rangle \tag{25}$$

where D is the elastic material matrix, α thermal expansion coefficients, d the strain-piezoelectric constants, T the temperature difference from the stress-free temperature, and $\mathcal{E}$ the electric field. The material coefficient matrices D, α, e are in general fully populated. However, if it is desired to model laminated smart composite shells in which each lamina exhibits a monoclinic symmetry about its own mid-surface and is rotated about the local normal to be a layer in the laminated shell, some elements of the material matrices will vanish for any value of the lay-up angle [14].

The virtual work of the mechanical loads can be obtained by introducing the virtual displacement as the Lagrangean variation of the real displacement field, such that

$$\delta\hat{\mathbf{R}} = \overline{\delta q}_{Bi}\mathbf{B}_i + x_3\delta\mathbf{B}_3 + \delta w_i\mathbf{B}_i + w_j\delta\mathbf{B}_j \tag{26}$$

where the virtual displacement of the reference surface is given by

$$\overline{\delta q}_{Bi} = \delta\mathbf{u} \cdot \mathbf{B}_i \tag{27}$$

and the virtual rotation of the reference surface is defined such that

$$\delta\mathbf{B}_i = (-\overline{\delta\psi}_{B\beta}\mathbf{B}_\beta \times \mathbf{B}_3 + \overline{\delta\psi}_{B3}\mathbf{B}_3) \times \mathbf{B}_i. \tag{28}$$

Since the strain is small, one may safely ignore products of the warping and the loading in the virtual rotation term. Then, the virtual work of the applied loads $\tau_i\mathbf{B}_i$ on the top surface, $\beta_i\mathbf{B}_i$ on the bottom surface, and body forces $\phi_i\mathbf{B}_i$ through the thickness is

$$\begin{aligned}\overline{\delta W} = {} & (\tau_i + \beta_i + \langle\phi_i\rangle)\overline{\delta q}_{Bi} + \delta(\tau_i w_i^+ + \beta_i w_i^- + \langle\phi_i w_i\rangle) \\ & + \overline{\delta\psi}_{B\alpha}\left[\frac{h}{2}(\tau_\alpha - \beta_\alpha) + \langle x_3\phi_\alpha\rangle\right]\end{aligned} \tag{29}$$

where τ_i, β_i, and ϕ_i are taken to be independent of the deformation, $()^+ = ()|_{x_3=\frac{h}{2}}$, and $()^- = ()|_{x_3=-\frac{h}{2}}$. By introducing column matrices $\overline{\delta q}$, $\overline{\delta\psi}$, τ, β, and ϕ, which are formed by stacking the three elements associated with indexed symbols of the same names, one may write the virtual work in a matrix form, so that

$$\overline{\delta W} = \overline{\delta q}^{\mathrm{T}} f + \overline{\delta\psi}^{\mathrm{T}} m + \delta(\tau^{\mathrm{T}} w^+ + \beta^{\mathrm{T}} w^- + \langle\phi^{\mathrm{T}} w\rangle) \tag{30}$$

where

$$\begin{aligned} f &= \tau + \beta + \langle\phi\rangle \\ m &= \begin{Bmatrix} \frac{h}{2}(\tau_1 - \beta_1) + \langle x_3\phi_1\rangle \\ \frac{h}{2}(\tau_2 - \beta_2) + \langle x_3\phi_2\rangle \\ 0 \end{Bmatrix}. \end{aligned} \tag{31}$$

Here, because the loading is of the order h/l or higher, to be consistent with our approximation we discard from the virtual work all corrections of the order of h/R. The complete statement of the problem can now be presented in terms of the principle of virtual work, such that

$$\delta U - \overline{\delta W} = 0. \tag{32}$$

We have three kinds of virtual quantities here: the virtual displacement $\overline{\delta q}$, the virtual rotation $\overline{\delta\psi}$, and the variation of warping field δw. The first two quantities will be handled by the 2D shell analysis [19]. Thus w is the only unknown quantity to be determined in the process of modeling. It can be observed that, in spite of the possibility of accounting for large displacements and rotations as well as nonconservative forces in the above, the problem that governs the warping is linear and conservative. Thus, one can pose the problem that governs the warping as the minimization of an energy functional

$$\delta\Pi = 0 \tag{33}$$

with

$$\Pi = U - (\tau^{\mathrm{T}} w^+ + \beta^{\mathrm{T}} w^- + \langle\phi^{\mathrm{T}} w\rangle). \tag{34}$$

What we have developed so far is the 3D displacement-based formulation for smart shells. However, this problem is still 3D and the difficulty of solving it will be comparable to that for any full 3D thermopiezoelasticity problem. Fortunately, the VAM can be used to calculate the 3D warping functions asymptotically to mitigate the difficulty associated with 3D problems.

3. Dimensional reduction

To rigorously reduce the original 3D problem to a 2D shell problem, one must attempt to reproduce the energy stored in the 3D structure in a 2D formulation. This dimensional reduction can only be done approximately, and one way to do it is by taking advantage of the smallness of h/l and h/R. To reduce the number of small parameters in the asymptotic analysis, it is desirable to assume that the strains caused by temperature and electricity are of the order ε. Thus the quantities of interest assume the following orders:

$$\begin{aligned} &\varepsilon_{\alpha\beta} \sim h\kappa_{\alpha\beta} \sim \varepsilon \qquad f_3 \sim \mu(h/l)^2\varepsilon \qquad f_\alpha \sim \mu(h/l)\varepsilon \\ &m_\alpha \sim \mu h(h/l)\varepsilon \qquad \alpha T \sim \varepsilon \qquad d\mathcal{E} \sim \varepsilon \end{aligned} \tag{35}$$

where μ represents the order of elastic material constants.

For the purpose of creating a shallow shell model of the Reissner–Mindlin type, we need to construct a model for piezoelectric shells with a 2D energy functional that is asymptotically correct up to $\mathrm{O}(h/R)$ and $\mathrm{O}(h^2/l^2)$, i.e.

$$\Pi = \mu\varepsilon^2\left[\mathrm{O}(1) + \mathrm{O}\left(\frac{h}{R}\right) + \mathrm{O}\left(\frac{h}{l}\right) + \mathrm{O}\left(\frac{h^2}{l^2}\right)\right]. \tag{36}$$

To deal with numerous layers and to be compatible with 2D finite element solvers, we use a separate 1D finite element discretization along the normal line to solve the minimization problem in the most economical manner, so that one can express the warping field as

$$w(x_i) = S(x_3)V(x_1, x_2) \tag{37}$$

where S is the shape function and V is the nodal value of warping field along the transverse normal. Substituting

equation (37) into (34), one can express the energy functional in a discretized form within the accuracy of our approximation, such that

$$\begin{aligned}2\Pi = {} & V^{\mathrm{T}}EV + 2V^{\mathrm{T}}(D_{h\epsilon}\epsilon + D_{Rh\epsilon}\epsilon + D_{hRh}V \\ & + D_{hR\epsilon}\epsilon + D_{hl_\alpha}V_{;\alpha}) + \epsilon^{\mathrm{T}}(D_{\epsilon\epsilon} + 2D_{\epsilon R\epsilon})\epsilon \\ & + V_{;\alpha}^{\mathrm{T}}D_{l_\alpha l_\beta}V_{;\beta} + 2V_{;\alpha}^{\mathrm{T}}D_{l_\alpha\epsilon}\epsilon - 2V^{\mathrm{T}}(\alpha_h + \alpha_{Rh}) \\ & - 2\epsilon^{\mathrm{T}}(\alpha_\epsilon + \alpha_{R\epsilon}) - 2V_{;\alpha}^{\mathrm{T}}\alpha_{l_\alpha} - 2V^{\mathrm{T}}(\mathcal{E}_h + \mathcal{E}_{Rh}) \\ & - 2\epsilon^{\mathrm{T}}(\mathcal{E}_\epsilon + \mathcal{E}_{R\epsilon}) - 2V_{;\alpha}^{\mathrm{T}}\mathcal{E}_{l_\alpha} + 2V^{\mathrm{T}}L \end{aligned} \tag{38}$$

where L contains the load related terms such that

$$L = -S^{+T}\tau - S^{-T}\beta - \langle S^{\mathrm{T}}\phi\rangle. \tag{39}$$

The new matrices carry the properties of both the geometry and material:

$$\begin{aligned} E &= \langle[\Gamma_h S]^{\mathrm{T}}D[\Gamma_h S]\rho\rangle & D_{h\epsilon} &= \langle[\Gamma_h S]^{\mathrm{T}}D\Gamma_\epsilon\rho\rangle \\ D_{hl_\alpha} &= \langle[\Gamma_h S]^{\mathrm{T}}D[\Gamma_{l_\alpha} S]\rangle & D_{l_\alpha l_\beta} &= \langle[\Gamma_{l_\alpha} S]^{\mathrm{T}}D[\Gamma_{l_\beta} S]\rangle \\ D_{\epsilon\epsilon} &= \langle\Gamma_\epsilon^{\mathrm{T}}D\Gamma_\epsilon\rho\rangle & D_{l_\alpha\epsilon} &= \langle[\Gamma_{l_\alpha} S]^{\mathrm{T}}D\Gamma_\epsilon\rangle \\ D_{hRh} &= \langle[\Gamma_h S]^{\mathrm{T}}D[\Gamma_{Rh} S]\rangle & D_{hR\epsilon} &= \langle[\Gamma_h S]^{\mathrm{T}}D\Gamma_{R\epsilon}\rangle \\ D_{Rh\epsilon} &= \langle[\Gamma_{Rh} S]^{\mathrm{T}}D\Gamma_\epsilon\rangle & D_{\epsilon R\epsilon} &= \langle\Gamma_\epsilon^{\mathrm{T}}D\Gamma_{R\epsilon}\rangle \\ \alpha_h &= \langle[\Gamma_h S]^{\mathrm{T}}D\alpha T\rho\rangle & \alpha_\epsilon &= \langle[\Gamma_\epsilon]^{\mathrm{T}}D\alpha T\rho\rangle \\ \alpha_{Rh} &= \langle[\Gamma_{Rh} S]^{\mathrm{T}}D\alpha T\rangle & \alpha_{R\epsilon} &= \langle[\Gamma_{R\epsilon}]^{\mathrm{T}}D\alpha T\rangle \\ \mathcal{E}_h &= \langle[\Gamma_h S]^{\mathrm{T}}Dd\mathcal{E}\rho\rangle & \mathcal{E}_\epsilon &= \langle[\Gamma_\epsilon]^{\mathrm{T}}Dd\mathcal{E}\rho\rangle \\ \mathcal{E}_{Rh} &= \langle[\Gamma_{Rh} S]^{\mathrm{T}}Dd\mathcal{E}\rangle & \mathcal{E}_{R\epsilon} &= \langle[\Gamma_{R\epsilon}]^{\mathrm{T}}Dd\mathcal{E}\rangle \\ \alpha_{l_\alpha} &= \langle[\Gamma_{l_\alpha} S]^{\mathrm{T}}D\alpha T\rangle & \mathcal{E}_{l_\alpha} &= \langle[\Gamma_{l_\alpha} S]^{\mathrm{T}}Dd\mathcal{E}\rangle. \end{aligned} \tag{40}$$

The discretized form of the constraints of warping functions, equation (12), can be written as

$$V^{\mathrm{T}}H\psi = 0 \tag{41}$$

where $H = \langle S^{\mathrm{T}}S\rangle$ and ψ is the normalized kernel matrix of E with zero initial curvatures such that $\psi^{\mathrm{T}}H\psi = I$. Our problem has now been transformed into the numerical minimization of equation (38) subject to constraints found in equation (41).

VAM requires one to find the leading terms of the functional according to the different orders. For the zeroth-order approximation, these leading terms associated with the unknown warping functions of equation (38) are

$$2\Pi_0^* = V^{\mathrm{T}}E_0V + 2V^{\mathrm{T}}D_{h\epsilon 0}\epsilon - 2V^{\mathrm{T}}\alpha_{h0} - 2V^{\mathrm{T}}\mathcal{E}_{h0} \tag{42}$$

where E_0, $D_{h\epsilon 0}$, α_{h0}, and $\mathcal{E}_{h0}$ are the corresponding matrices defined in equation (40) with $\rho = 1$ (no geometrical correction). The zeroth-order warping functions that minimize equation (42) are

$$V_0 = \hat{V}_0\epsilon + V_{\mathrm{T}} + V_{\mathcal{E}}. \tag{43}$$

Substituting equation (43) back into equation (38), one can obtain a 2D electric enthalpy asymptotically correct through the order of $\mu\varepsilon^2$ as

$$2\Pi_0 = \epsilon^{\mathrm{T}}A\epsilon - 2\epsilon^{\mathrm{T}}N_{\mathrm{T}} - 2\epsilon^{\mathrm{T}}N_{\mathcal{E}} \tag{44}$$

with

$$\begin{aligned} A &= \hat{V}_0^{\mathrm{T}}D_{h\epsilon 0} + D_{\epsilon\epsilon 0} \\ N_{\mathrm{T}} &= \alpha_{\epsilon 0} + \tfrac{1}{2}(\hat{V}_0{}^{\mathrm{T}}\alpha_{h0} - D_{h\epsilon 0}^{\mathrm{T}}V_{\mathrm{T}}) \\ N_{\mathcal{E}} &= \mathcal{E}_{\epsilon 0} + \tfrac{1}{2}(\hat{V}_0{}^{\mathrm{T}}\mathcal{E}_{h0} - D_{h\epsilon 0}^{\mathrm{T}}V_{\mathcal{E}}) \end{aligned} \tag{45}$$

where A is the 2D stiffness matrix and N_{T} and $N_{\mathcal{E}}$ are non-mechanical stress resultants due to given temperature and electric fields, respectively. Although the energy of this approximation coincides with classical laminated piezoelectric shell theories, we do not invoke the Kirchhoff–Love assumption to obtain this result. The result is the same as the zeroth-order approximation of piezoelectric plate theory [14] because the geometrical correction due to the initial curvatures has not been included yet.

Although a shell theory based on this zeroth-order approximation can do a good job in predicting the global deformation and in-plane quantities for thin structures, refined theories taking advantage of small parameters h/R and h/l are required for moderately thick shells to give a better prediction of global deformation, in-plane quantities, and especially out-of-plane stresses and strains (σ_{i3}, Γ_{i3}). Let us obtain the correction coming from h/R first to include the effect of initial curvatures. Since we are only interested in obtaining an enthalpy that is asymptotically correct up to the first order of h/R, which is sufficient for most engineering applications, it is unnecessary to calculate the refined warping with respect to h/R because it makes no contribution to the enthalpy up to the first order of h/R. At this stage we will postpone the consideration of the mechanical load contribution to the step where the h/l correction is determined. The enthalpy, asymptotically correct up to the order of h/R, can be expressed as

$$2\Pi_R = \epsilon^{\mathrm{T}}A_R\epsilon - 2\epsilon^{\mathrm{T}}N_{TR} - 2\epsilon^{\mathrm{T}}N_{\mathcal{E}_R} \tag{46}$$

with

$$\begin{aligned} A_R = {} & A + \hat{V}_0^{\mathrm{T}}E^*\hat{V}_0 + D_{\epsilon\epsilon}^* + 2\hat{V}_0^{\mathrm{T}}(D_{h\epsilon}^* + D_{hR\epsilon} + D_{Rh\epsilon}) \\ & + 2D_{\epsilon R\epsilon} + \hat{V}_0^{\mathrm{T}}(D_{hRh} + D_{hRh})\hat{V}_0 \\ N_{TR} = {} & N_{\mathrm{T}} + \alpha_\epsilon^* + \alpha_{R\epsilon} - (D_{h\epsilon}^* + D_{hR\epsilon} + D_{Rh\epsilon})^{\mathrm{T}}V_{\mathrm{T}} \\ & + \hat{V}_0^{\mathrm{T}}\left[\alpha_{Rh} + \alpha_h^* - (E^* + D_{hRh} + D_{hRh}^{\mathrm{T}})V_{\mathrm{T}}\right] \\ N_{\mathcal{E}R} = {} & N_{\mathcal{E}} + \mathcal{E}_\epsilon^* + \mathcal{E}_{R\epsilon} - (D_{h\epsilon}^* + D_{hR\epsilon} + D_{Rh\epsilon})^{\mathrm{T}}V_{\mathcal{E}} \\ & + \hat{V}_0^{\mathrm{T}}\left[\mathcal{E}_{Rh} + \mathcal{E}_h^* - (E^* + D_{hRh} + D_{hRh}^{\mathrm{T}})V_{\mathcal{E}}\right]. \end{aligned} \tag{47}$$

All the starred matrices are defined according to equation (40) with ρ replaced by $\rho - 1$.

To account for transverse shear deformation, one needs to find an energy that is asymptotically correct through the order of $(h/l)^2$ relative to the leading terms. This refinement needs to calculate the refined warping field of the order of h/l. Perturbing the zeroth-order warping with V_1, which is of the order of $(h/l)V_0$, one obtains:

$$V = V_0 + V_1. \tag{48}$$

Substituting equation (48) back into equation (38), one can obtain the leading terms for the first-order approximation as

$$2\Pi_1^* = V_1^{\mathrm{T}}EV_1 + 2V_1^{\mathrm{T}}D_\alpha\epsilon_{;\alpha} + 2V_1TL_{\mathrm{T}} + 2V_1L_{\mathcal{E}} + 2V_1^{\mathrm{T}}L \tag{49}$$

where

$$D_\alpha = (D_{hl_\alpha} - D_{\hat{h}l_\alpha}^{\mathrm{T}})\hat{V}_0 - D_{l_\alpha\epsilon}$$
$$L_{\mathrm{T}} = (D_{hl_\alpha} - D_{\hat{h}l_\alpha}^{\mathrm{T}})V_{\mathrm{T};\alpha} + \alpha_{l_\alpha;\alpha} \tag{50}$$
$$L_{\mathcal{E}} = (D_{hl_\alpha} - D_{\hat{h}l_\alpha}^{\mathrm{T}})V_{\mathcal{E};\alpha} + \mathcal{E}_{l_\alpha;\alpha}.$$

It is understood that the order of the loads in equation (35) is associated with warping functions of different orders [11]. Integration by parts with respect to the in-plane coordinates is used here and hereafter whenever it is convenient for the derivation, because our goal is to obtain an interior solution for the shell without considering edge effects. The energy functional will be consistently kept within the accuracy of approximation, equation (36).

The first-order warping can be solved as

$$V_1 = V_{1\alpha}\epsilon_{;\alpha} + V_{1T} + V_{1\mathcal{E}} + V_{1L}. \tag{51}$$

Finally, we obtain a total enthalpy that is asymptotically correct up to the order of $\mu\varepsilon(h/l)^2$ and $\mu\varepsilon h/R$, given by

$$\begin{aligned} 2\Pi_1 = {} & \epsilon^{\mathrm{T}} A_R \epsilon + \epsilon_{;1}^{\mathrm{T}} B \epsilon_{;1} + 2\epsilon_{;1}^{\mathrm{T}} C \epsilon_{;2} + \epsilon_{;2}^{\mathrm{T}} \mathcal{D} \epsilon_{;2} \\ & - 2\epsilon^{\mathrm{T}} F_{\mathrm{T}} - 2\epsilon^{\mathrm{T}} F_{\mathcal{E}} - 2\epsilon^{\mathrm{T}} F \end{aligned} \tag{52}$$

where

$$\begin{aligned} B &= \hat{V}_0^{\mathrm{T}} D_{l_1 l_1} \hat{V}_0 + V_{11}^{\mathrm{T}} D_1 \\ C &= \hat{V}_0^{\mathrm{T}} D_{l_1 l_2} \hat{V}_0 + \tfrac{1}{2}(V_{11}^{\mathrm{T}} D_2 + D_1^{\mathrm{T}} V_{12}) \\ \mathcal{D} &= \hat{V}_0^{\mathrm{T}} D_{l_2 l_2} \hat{V}_0 + V_{12}^{\mathrm{T}} D_2 \\ F &= \tfrac{1}{2}(D_\alpha^{\mathrm{T}} V_{1L;\alpha} + V_{1\alpha}^{\mathrm{T}} L_{;\alpha}) - \hat{V}_0^{\mathrm{T}} L \end{aligned} \tag{53}$$

with the non-mechanical load due to temperature

$$F_{\mathrm{T}} = N_{TR} + \hat{V}_0^{\mathrm{T}} D_{l_\alpha l_\beta} V_{\mathrm{T};\alpha\beta} + \tfrac{1}{2}(V_{1\alpha}^{\mathrm{T}} L_{\mathrm{T};\alpha} + D_\alpha^{\mathrm{T}} V_{1T;\alpha}) \tag{54}$$

and the non-mechanical load due to electric field

$$\begin{aligned} F_{\mathcal{E}} = {} & N_{\mathcal{E}R} - \hat{V}_0^{\mathrm{T}} D_{hl_\alpha} V_{\mathcal{E};\alpha} - D_{l_\alpha\mathcal{E}}^{\mathrm{T}} V_{\mathcal{E};\alpha} \\ & + \hat{V}_0^{\mathrm{T}} D_{l_\alpha l_\beta} V_{\mathcal{E};\alpha\beta} + \tfrac{1}{2}(V_{1\alpha}^{\mathrm{T}} L_{\mathcal{E};\alpha} + D_\alpha^{\mathrm{T}} V_{1\mathcal{E};\alpha}). \end{aligned} \tag{55}$$

Here, the monoclinic symmetry has already been used to obtain the asymptotically correct energy in equation (52). The applied mechanical loads, temperature, and electric field should not vary rapidly over the shell surface, so that F, F_{T}, and $F_{\mathcal{E}}$ will be of the desired orders to meet the requirement of asymptotical correctness.

4. Constructing the Reissner–Mindlin model

Although equation (52) is asymptotically correct to $\mathrm{O}(h^2/l^2)$ and $\mathrm{O}(h/R)$, it is difficult to use it directly because more complicated boundary conditions than necessary have to be introduced. To obtain an energy functional that is of practical use, one can transform the present approximation into the Reissner–Mindlin form, a commonly used model in practice.

In the Reissner–Mindlin model, there are two additional degrees of freedom—the transverse shear strains. These are incorporated into the rotation of a local line element through the thickness. If we introduce another triad $\mathbf{B}_i^*$ for the deformed Reissner–Mindlin shell, the definition of 2D strains becomes

$$\mathbf{R}_{,\alpha} = A_\alpha(\mathbf{B}_\alpha^* + \varepsilon_{\alpha\beta}^*\mathbf{B}_\beta^* + 2\gamma_{\alpha 3}\mathbf{B}_3^*) \tag{56}$$

$$\mathbf{B}_{i,\alpha}^* = A_\alpha(-K_{\alpha 2}^*\mathbf{B}_1^* + K_{\alpha 1}^*\mathbf{B}_2^* + K_{\alpha 3}^*\mathbf{B}_3^*) \times \mathbf{B}_i^* \tag{57}$$

where $\gamma = \lfloor\, 2\gamma_{13} \quad 2\gamma_{23} \,\rfloor^{\mathrm{T}}$. Since $\mathbf{B}_i^*$ is uniquely determined by $\mathbf{B}_i$ and γ, one can derive the following kinematic identity between the strain measures $\mathcal{R}$ of the Reissner–Mindlin shell and ϵ:

$$\epsilon = \mathcal{R} - \mathcal{D}_\alpha\gamma_{;\alpha} \tag{58}$$

where

$$\begin{aligned} \mathcal{D}_1 &= \begin{bmatrix} 0 & 0 & 0 & 1 & 0 & 0 \\ 0 & 0 & 0 & 0 & 1 & 0 \end{bmatrix}^{\mathrm{T}} \\ \mathcal{D}_2 &= \begin{bmatrix} 0 & 0 & 0 & 0 & 1 & 0 \\ 0 & 0 & 0 & 0 & 0 & 1 \end{bmatrix}^{\mathrm{T}} \\ \mathcal{R} &= \lfloor\, \varepsilon_{11}^* \quad 2\varepsilon_{12}^* \quad \varepsilon_{22}^* \quad \kappa_{11}^* \quad \kappa_{12}^* + \kappa_{21}^* \quad \kappa_{22}^* \,\rfloor^{\mathrm{T}}. \end{aligned} \tag{59}$$

Now one can rewrite the strain energy expressed in equation (52), correct to the orders of interest according to equation (36), in terms of strains of the Reissner–Mindlin model as

$$\begin{aligned} 2\Pi_1 = {} & \mathcal{R}^{\mathrm{T}} A_R \mathcal{R} - 2\mathcal{R}^{\mathrm{T}} A \mathcal{D}_\alpha \gamma_{;\alpha} + \mathcal{R}_{;1}^{\mathrm{T}} B \mathcal{R}_{;1} \\ & + 2\mathcal{R}_{;1}^{\mathrm{T}} C \mathcal{R}_{;2} + \mathcal{R}_{;2}^{\mathrm{T}} D \mathcal{R}_{;2} \\ & - 2\mathcal{R}^{\mathrm{T}}(F_{\mathrm{T}} + F_{\mathcal{E}} + F) + 2\gamma_{;\alpha}^{\mathrm{T}} \mathcal{D}_\alpha^{\mathrm{T}}(N_{\mathrm{T}} + N_{\mathcal{E}}). \end{aligned} \tag{60}$$

A generalized Reissner–Mindlin model of practical use can be of the form

$$2\Pi_{\mathcal{R}} = \mathcal{R}^{\mathrm{T}} A_R \mathcal{R} + \gamma^{\mathrm{T}} G \gamma - 2\mathcal{R}^{\mathrm{T}} F_{\mathcal{R}} - 2\gamma^{\mathrm{T}} F_\gamma. \tag{61}$$

To find an equivalent Reissner–Mindlin model for equation (60), one has to eliminate all partial derivatives of the classical 2D strain measures $\mathcal{R}_{;\alpha}$. The equilibrium equations in [19] are used to achieve this purpose. From the two equilibrium equations balancing bending moments with applied moments m_α, one can obtain the following formula:

$$G\gamma - F_\gamma = \mathcal{D}_\alpha^{\mathrm{T}}(A\mathcal{R}_{;\alpha} - F_{\mathcal{R};\alpha}) + \lfloor\, m_1 \quad m_2 \,\rfloor^{\mathrm{T}}. \tag{62}$$

Using equation (62), one can rewrite equation (60) as

$$2\Pi_1 = 2\Pi_{\mathcal{R}} + U^* \tag{63}$$

where

$$U^* = \mathcal{R}_{;1}^{\mathrm{T}} \overline{B} \mathcal{R}_{;1} + 2\mathcal{R}_{;1}^{\mathrm{T}} \overline{C} \mathcal{R}_{;2} + \mathcal{R}_{;2}^{\mathrm{T}} \overline{D} \mathcal{R}_{;2} \tag{64}$$

and

$$\begin{aligned} F_{\mathcal{R}} &= F_{\mathrm{T}} + F_{\mathcal{E}} + F \\ F_\gamma &= \mathcal{D}_\alpha^{\mathrm{T}}(N_{\mathrm{T};\alpha} + N_{\mathcal{E};\alpha}) \\ \overline{B} &= B + A\mathcal{D}_1 G^{-1} \mathcal{D}_1^{\mathrm{T}} A \\ \overline{C} &= C + A\mathcal{D}_1 G^{-1} \mathcal{D}_2^{\mathrm{T}} A \\ \overline{D} &= D + A\mathcal{D}_2 G^{-1} \mathcal{D}_2^{\mathrm{T}} A. \end{aligned} \tag{65}$$

If we can drive U^* to zero for any $\mathcal{R}$, then we have found an asymptotically correct Reissner–Mindlin shell model. For generally anisotropic shells, this term will not be zero; but we can minimize the error to obtain a Reissner–Mindlin model that is as close to asymptotical correctness as possible. The accuracy of the Reissner–Mindlin model depends on how close to zero one can drive this term of the energy.

One could proceed with the optimization at this point, but there are only three unknowns, the elements of the shear stiffness matrix G. It is desirable to introduce more unknowns, if possible, into the optimization problem. It is known that there is no unique shell theory of a given order [20]. One can relax the constraints in equation (12) to be $\langle w_i \rangle$ = constant and still obtain an asymptotically correct enthalpy. Since the zeroth-order approximation gives us an asymptotic model corresponding to classical shell theory, we only relax the constraints for the first-order approximation. This relaxation will modify the warping field to be

$$\overline{V}_1 = (V_{1\alpha} + L_\alpha)\epsilon_{;\alpha} + V_{1T} + V_{1\mathcal{E}} + V_{1L} \tag{66}$$

where L_α consists of 24 constants. The remaining energy U^* will also be modified to be

$$U^* = \mathcal{R}_{;1}^{\mathrm{T}} \hat{B} \mathcal{R}_{;1} + 2\mathcal{R}_{;1}^{\mathrm{T}} \hat{C} \mathcal{R}_{;2} + \mathcal{R}_{;2}^{\mathrm{T}} \hat{D} \mathcal{R}_{;2} \tag{67}$$

and

$$\begin{aligned} \hat{B} &= \overline{B} + 2L_1^{\mathrm{T}} D_1 \\ \hat{C} &= \overline{C} + (L_1^{\mathrm{T}} D_2 + D_1^{\mathrm{T}} L_2) \\ \hat{D} &= \overline{D} + 2L_2^{\mathrm{T}} D_2. \end{aligned} \tag{68}$$

Since now we have 27 unknowns, the optimization is much more flexible. It can give us a more optimal solution for the shear stiffness matrix G to fit the asymptotically correct enthalpy into the Reissner–Mindlin model, and after minimizing U^*, the 'best' Reissner–Mindlin model, from the asymptotic point of view, to be used for 2D shell analysis will be achieved. The model is mathematically represented in equation (61), with A_R, G, $F_{\mathcal{R}}$, and F_γ capturing the material and geometric information eliminated in the reduced 2D analysis.

5. Recovery relations

From the above, we have obtained a Reissner–Mindlin piezoelectric shell model which is as close as possible to being asymptotically correct in the sense of matching the total electric enthalpy. The constitutive model can be used as input for a shell theory derived from the 2D enthalpy in equation (61).

In many applications, however, while it is necessary to accurately calculate the 2D displacement field of smart composite shells, this is not sufficient. Ultimately, the fidelity of a reduced-order model depends on how well it can predict the 3D results in the original 3D structure. Hence recovery relations should be provided to complete the reduced-order model. By recovery relations, we mean expressions for 3D displacement, strain, and stress fields in terms of 2D quantities and the coordinate x_3.

For an enthalpy that is asymptotically correct up to $\mathrm{O}(h/R)$ and $\mathrm{O}(h^2/l^2)$, we can recover the 3D fields which include all the terms of the first order of h/l, and part of the terms of the first order of h/R that contribute to the enthalpy of the first order of h/R. Using equations (1), (10), and (11), one can recover the 3D displacement field as

$$U_{3\mathrm{D}} = u_{2\mathrm{D}} + x_3 \lfloor C_{31} \quad C_{32} \quad C_{33} - 1 \rfloor^{\mathrm{T}} + SV_0 + S\overline{V}_1 \tag{69}$$

where $U_{3\mathrm{D}}$ is the column matrix of 3D displacements and $u_{2\mathrm{D}}$ is the shell displacements. C_{ij} are components of the global rotation tensor from equation (10). The recovered 3D strain field can be calculated using equation (18), such that

$$\Gamma = \Gamma_h S(V_0 + \overline{V}_1) + \Gamma_\epsilon \epsilon + \Gamma_{l_\alpha} S V_{0\alpha} + \Gamma_{Rh} V_0 + \Gamma_{R\epsilon} \epsilon. \tag{70}$$

Then, one can use the 3D constitutive law to obtain 3D stresses σ_{ij}. In view of the fact that the initial curvatures of the shell only correct the enthalpy related to the classical strain measures, we will delete the effects of initial curvatures in the recovery of the transverse stresses so that the 3D enthalpy due to transverse stresses corresponds to the 2D enthalpy due to transverse shear deformation.

In contrast to conventional FOSDT, the present analysis calculates an optimum shear stiffness matrix G without introducing so-called shear correction factors. The recovered 3D results, especially the transverse shear stresses, are much better than those from FOSDT. However, the recovered transverse normal stress is not as accurate as the other components because the transverse normal stress is a second-order quantity and its contribution to the energy functional is not included in the Reissner–Mindlin model. Thus, in order to obtain recovery relations that are valid to the same order as the energy, the VAM iteration needs to be applied one more time to obtain an energy functional of $\mathrm{O}(h^4/l^4)$, which is not used in the modeling but only to correct the recovering relations. This approach has proved to be successful for various plate models [11, 13, 14]. However, it is doubtful that this approach can be applied for shells. Such an extension would imply $h/R \ll h^4/l^4$, which in turn implies an extremely small value for h/R and thus negligible geometric corrections to the energy functional. Such a shell structure could be confidently analyzed using a plate stiffness model along with a 2D shell analysis. We attempted to obtain a reasonable recovery for the transverse normal stress this way in [12] by tuning the small parameters h/l and h/R, which reduces the range of applicability for the developed theory. It will be shown later by numerical examples that this approach may fail for the general case. The ideal solution is to develop a complete second-order theory in terms of h/R and h/l so that the transverse normal stress can be recovered accurately for realistic cases. This is a monumental task and is outside the scope of the present paper.

6. Numerical examples

The present theory has been implemented in VAPAS. To compare the present theory with exact 3D solutions, we investigate several cases for cylindrical bending of piezoelectric composite shells. All the distributions of 3D stresses through the thickness are compared with CLT, FOSDT, and 3D exact solutions [21] specialized for prescribed temperature and electric fields.

The structure analyzed is a four-layer smart cylindrical shell with $h = 1$ mm, $R = 10$ mm, and $\varphi = \frac{\pi}{3}$ (see figure 2). The coordinates are chosen in such a way that $x_1 \in [0, \varphi]$, $x_2 \in [0, \infty)$, and $x_3 \in [-h/2, h/2]$. The two face sheets are made with piezoelectric material with properties given by

$$E_L = E_{\mathrm{T}} = 63 \text{ GPa} \qquad G_{LT} = G_{TT} = 24.6 \text{ GPa}$$

$$\nu_{LT} = \nu_{TT} = 0.28 \qquad d_{113} = d_{223} = 150 \times 10^{-12} \text{ m V}^{-1}.$$

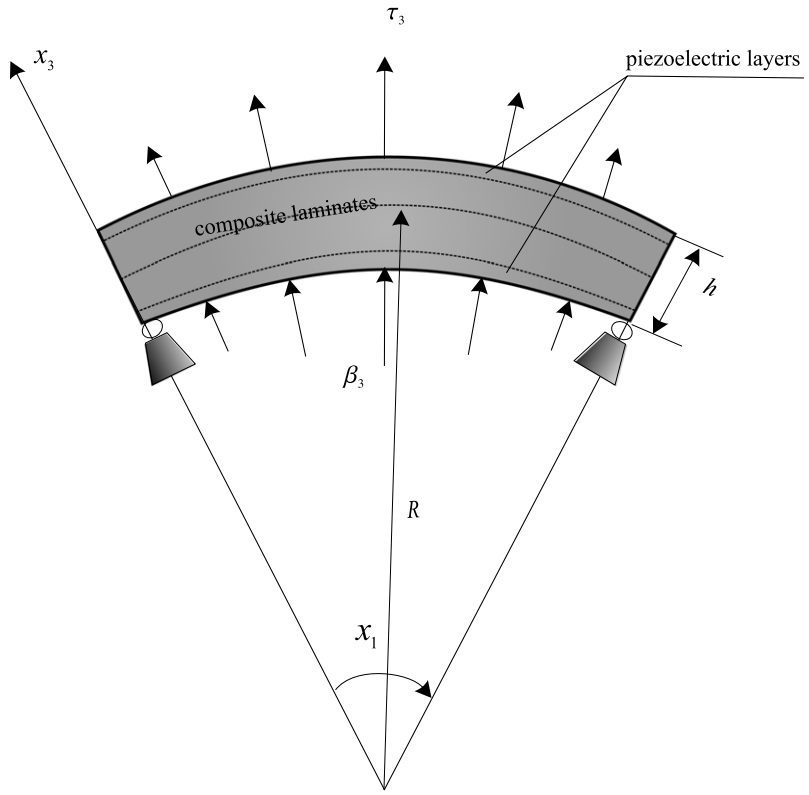

Figure 2. Sketch of a four-layer smart shell: simply supported infinitely long cylindrical shell.

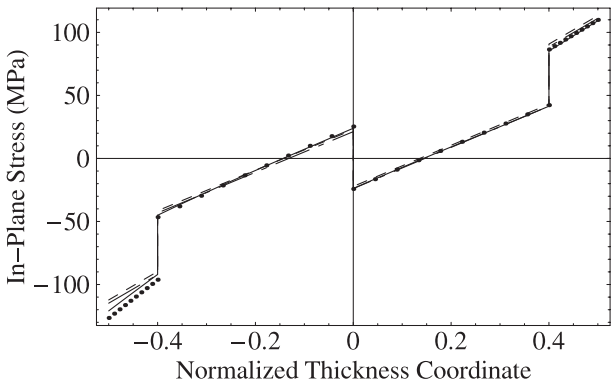

Figure 3. Distribution of the 3D stress σ_{11}. Solid line, exact solution; dots, VAPAS; dashed line, FOSDT; long-dash/short-dash line, CLT.

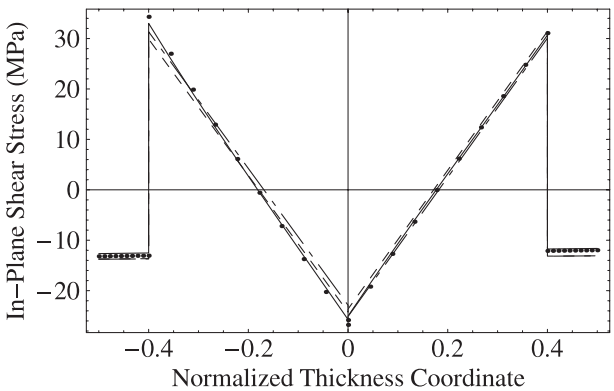

Figure 4. Distribution of the 3D stress σ_{12}. Solid line, exact solution; dots, VAPAS; dashed line, FOSDT; long-dash/short-dash line, CLT.

The inside layers are normal graphite/epoxy composites with the following properties:

$$E_L = 172 \text{ GPa} \qquad E_T = 6.9 \text{ GPa} \qquad G_{LT} = 3.4 \text{ GPa}$$

$$G_{TT} = 1.4 \text{ GPa} \qquad \nu_{LT} = 0.25 \qquad \nu_{TT} = 0.25.$$

The piezoelectric layers are each 0.1 mm thick, and the regular composite layers are each 0.4 mm thick. The lay-up scheme is [0°/−45°/45°/0°] from bottom to top.

We first investigate the case when this smart shell is subject to surface mechanical loads

$$\tau_3 = \beta_3 = \tfrac{1}{2}\sin(3x_1) \text{ N mm}^{-2}. \tag{71}$$

The recovered stresses are plotted in figures 3–8, where the solid line represents the results from exact solution, the dotted line from VAPAS, the dashed line from FOSDT, and the long-dash/short-dash line from CLT. Note that because $\sigma_{\alpha\beta}$ and σ_{33} are sine functions of x_1 they are plotted at $x_1 = \pi/6$, while $\sigma_{\alpha 3}$ are cosine functions of x_1 and are plotted at $x_1 = 0$ or $x_1 = \pi/3$. The results show excellent agreement between VAPAS and the exact solution, the only exception being the transverse normal stress. The recovered transverse shear and normal stresses satisfy the boundary and continuity conditions on the interfaces of the different layers, which was not the case in [12]. The reason for this improvement is that we have here limited the effects of initial curvatures in the recovering relations to the in-plane components. VAPAS fails to predict

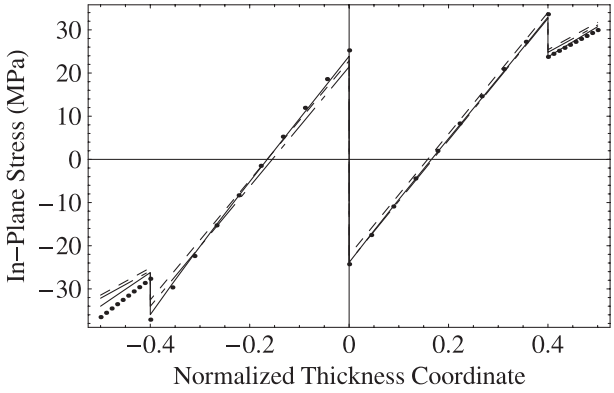

Figure 5. Distribution of the 3D stress σ_{22}. Solid line, exact solution; dots, VAPAS; dashed line, FOSDT; long-dash/short-dash line, CLT.

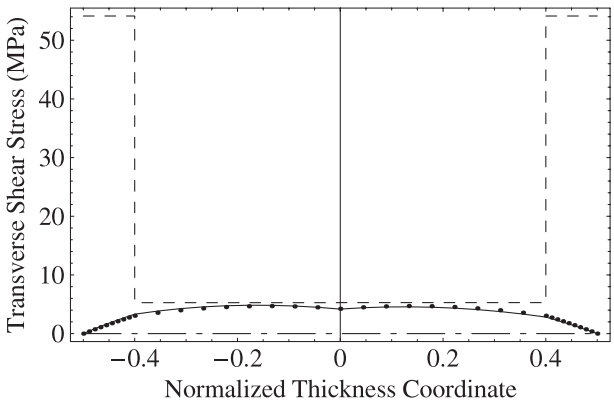

Figure 6. Distribution of the 3D stress σ_{13}. Solid line, exact solution; dots, VAPAS; dashed line, FOSDT; long-dash/short-dash line, CLT.

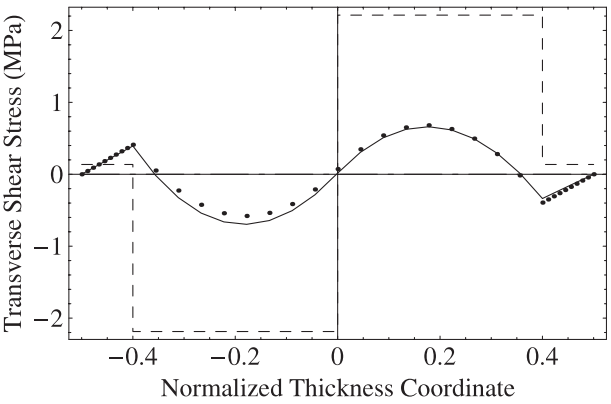

Figure 7. Distribution of the 3D stress σ_{23}. Solid line, exact solution; dots, VAPAS; dashed line, FOSDT; long-dash/short-dash line, CLT.

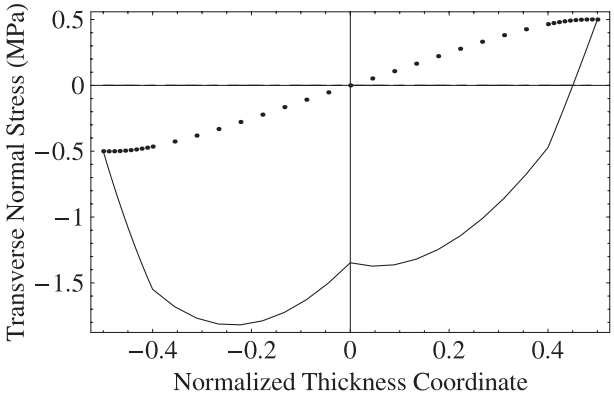

Figure 8. Distribution of the 3D stress σ_{33}. Solid line, exact solution; dots, VAPAS; dashed line, FOSDT; long-dash/short-dash line, CLT.

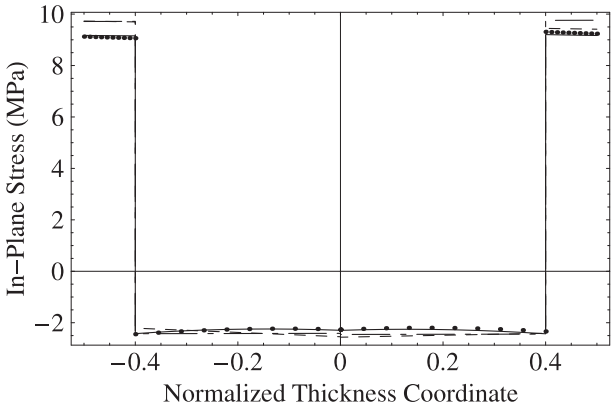

Figure 9. Distribution of the 3D stress σ_{11}. Solid line, exact solution; dots, VAPAS; dashed line, FOSDT; long-dash/short-dash line, CLT.

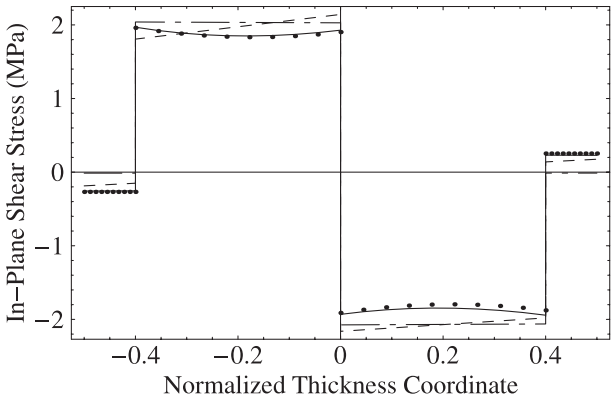

Figure 10. Distribution of the 3D stress σ_{12}. Solid line, exact solution; dots, VAPAS; dashed line, FOSDT; long-dash/short-dash line, CLT.

an accurate transverse normal stress for this case because it involves a significant contribution from the initial curvatures. It is somewhat relieving to note that transverse normal stresses are typically much smaller than other components. For the later cases, we will not show the results for this component.

The second case is to study the stress distribution due to prescribed electric potential without applied mechanical loads. We assume the lower surfaces of the piezoelectric layers are grounded and an electric potential $\phi = 100\sin(3x_1)$ is applied to the upper surfaces of both piezoelectric layers. The 3D stress distribution through the thickness is plotted in figures 9–13. One can observe from these plots that not only are the in-plane components from VAPAS almost on top of the exact 3D solutions, but also the transverse shear stresses from VAPAS are very close to those from the exact solution. These results demonstrate that VAPAS can provide very accurate predictions

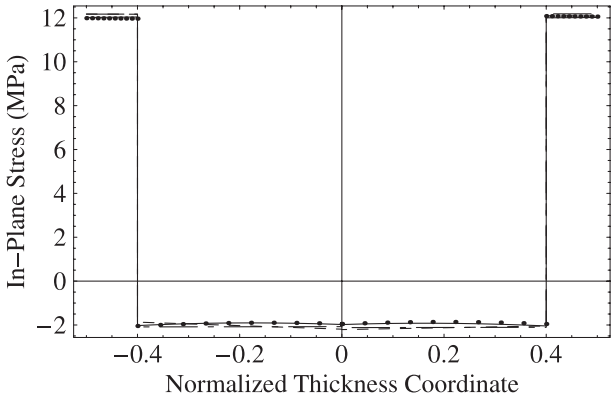

Figure 11. Distribution of the 3D stress σ_{22}. Solid line, exact solution; dots, VAPAS; dashed line, FOSDT; long-dash/short-dash line, CLT.

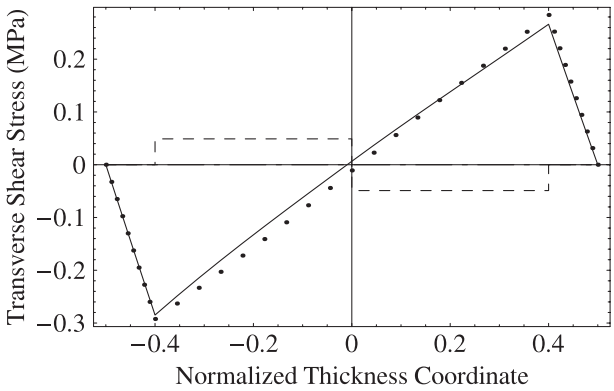

Figure 12. Distribution of the 3D stress σ_{13}. Solid line, exact solution; dots, VAPAS; dashed line, FOSDT; long-dash/short-dash line, CLT.

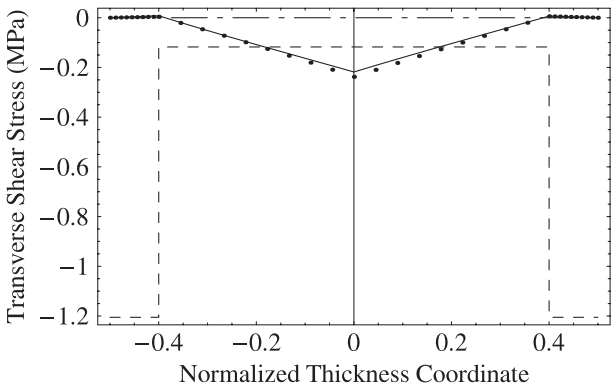

Figure 13. Distribution of the 3D stress σ_{23}. Solid line, exact solution; dots, VAPAS; dashed line, FOSDT; long-dash/short-dash line, CLT.

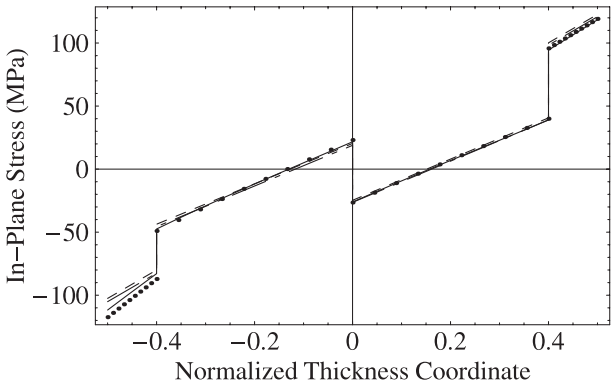

Figure 14. Distribution of the 3D stress σ_{11}. Solid line, exact solution; dots, VAPAS; dashed line, FOSDT; long-dash/short-dash line, CLT.

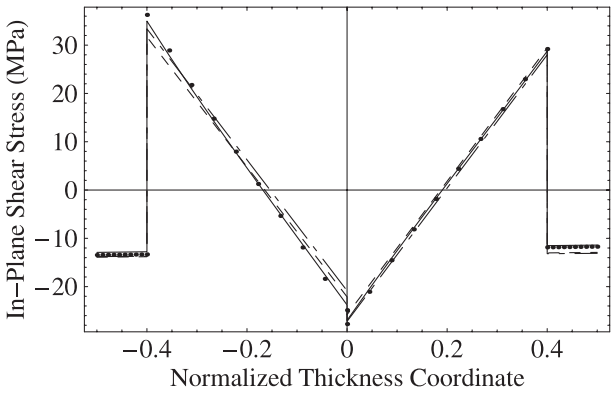

Figure 15. Distribution of the 3D stress σ_{12}. Solid line, exact solution; dots, VAPAS; dashed line, FOSDT; long-dash/short-dash line, CLT.

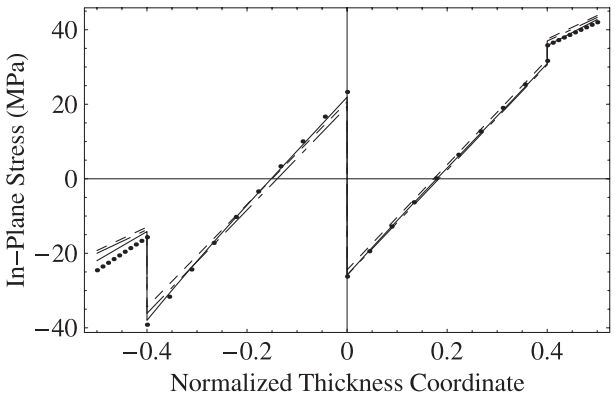

Figure 16. Distribution of the 3D stress σ_{22}. Solid line, exact solution; dots, VAPAS; dashed line, FOSDT; long-dash/short-dash line, CLT.

for the stresses (except the transverse normal stress) induced by the prescribed electric field.

The last example is to calculate the stresses produced in the structure due to both a prescribed electric potential and applied mechanical loads. The recovered stress distributions through the thickness for this case are plotted in figures 14–18. Again, very good agreement between the exact solution and VAPAS is observed. Mathematically, this case is a linear superposition of the previous two cases, since we have used linear theory for the purpose of validation. However, VAPAS is by no means restricted to linear theories. Similar accuracy is also achieved for combined thermal, electric, and mechanical loads; for the sake of brevity, such cases are not presented here. Although the results from CLT and FOSDT have reasonable agreement with the exact solution for the in-plane components, the transverse shear stresses are not available from CLT, and the values obtained from FOSDT are unacceptable.

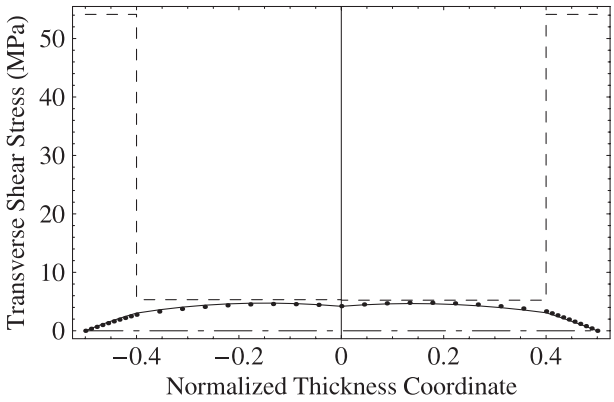

Figure 17. Distribution of the 3D stress σ_{13}. Solid line, exact solution; dots, VAPAS; dashed line, FOSDT; long-dash/short-dash line, CLT.

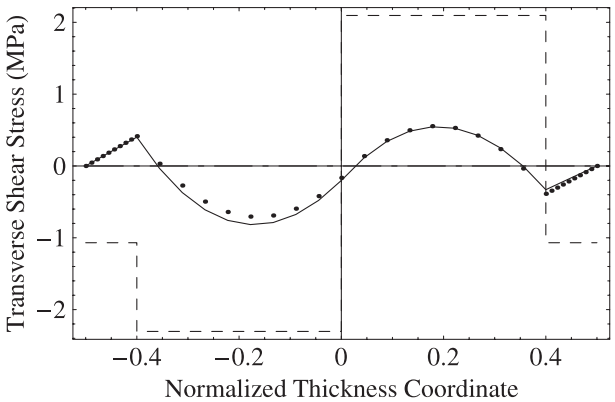

Figure 18. Distribution of the 3D stress σ_{23}. Solid line, exact solution; dots, VAPAS; dashed line, FOSDT; long-dash/short-dash line, CLT.

7. Conclusions

A Reissner–Mindlin model for piezoelectric composite shells has been developed to analyze one-way coupled thermopiezoelastic behavior. The variational-asymptotic method has been used to mathematically split the original 3D problem into a 1D through-the-thickness analysis and a 2D shell analysis. The through-the-thickness analysis provides a 2D electric enthalpy including both geometric and shear refinements for the 2D shell analysis. Although the present analysis reduces to the form of a simple Reissner–Mindlin model, numerical results have shown that it very accurately approximates the original 3D model.

The main attributes of the developed model are the following.

(i) The dimensional reduction from the 3D representation is carried out rigorously using the variational-asymptotic method, without invoking ad hoc kinematical assumptions.

(ii) The formulation is intrinsic and suitable for both geometrically linear and nonlinear shell analysis.

(iii) The Reissner–Mindlin model developed in this work is *not* a first-order shear-deformation theory. The present model, using 3D warping functions, incorporates all possible deformations, including those that are purposely eliminated from first-order shear-deformation theories.

(iv) The present theory decouples the modelling process of the shell completely from the 2D shell analysis over the reference surface, so that the 2D generalized constitutive model obtained can be used as an input for general 2D shell solvers. The ease with which VAPAS may be connected to 2D shell solvers and the confidence one can have in the accuracy of the recovered stress and strain allow the structural analyst focus on solving the 2D problem for different situations.

The computer program VAPAS can now be used along with a 2D Reissner–Mindlin type shell solver to perform an efficient yet accurate analysis for thermopiezoelastic behavior of piezoelectric composite shells. Such a tool is very useful for designers to carry out accurate trade-off studies more efficiently. To be compatible with the present model, the shell solver should be able to use a stiffness matrix of the form of our generalized Reissner–Minlin model as input and have a similar definition of shell strains. The multi-flexible-body dynamic simulation code DYMORE [22] is such an example.

It is noticed that the present work only deals with thermal and/or piezoelectric actuation of piezoelectric composite shells within the range of linear material relations. Changes of thermal and electric fields caused by deformation of the smart shell and material nonlinearity cannot be treated by the present theory. Such an extension is possible but requires significant effort. One needs to incorporate the electric potential and temperature as fundamental variables, which means one needs to carry out the asymptotic expansion for mechanical variables, the electric potential, and temperature by calculating the corresponding warping functions for different types of variables.

References

[1] Saravanos D A and Heyliger P R 1999 Mechanics and computational models for laminated piezoelectric beams, plates, and shells *Appl. Mech. Rev.* **52** 305–19

[2] Giurgiutiu V 2000 Review of smart materials actuation solutions for aeroelastic and vibration control *J. Intell. Mater. Syst. Struct.* **11** 525–44

[3] Chopra I 2002 Review of state of art of smart structures and integrated systems *AIAA J.* **40** 2145–87

[4] Tauchert T R 1992 Piezothermoelastic behavior of a laminated plate *J. Therm. Stresses* **15** 25–37

[5] Lee H-J and Saravanos D A 1997 Generalized finite element formulation for smart multilayered thermal piezoelectric composite plates *Int. J. Solids Struct.* **34** 3355–71

[6] Chattopadhyay A, Li J and Gu H 1999 Coupled thermo-piezoelectric-mechanical model for smart composite laminates *AIAA J.* **37** 1633–8

[7] Lee C K 1990 Theory of laminated piezoelectric plates for the design of distributed sensors/actuators *J. Acoust. Soc. Am.* **87** 1144–58

[8] Tzou H S and Zhong J P 1993 Electromechanics and vibrations of piezoelectric shell distributed systems *J. Dyn. Syst. Meas. Control* **115** 506–17

[9] Oh J and Cho M 2004 A finite element based on cubic zig-zag plate theory for the prediction of thermo-electric-mechanical behaviors *Int. J. Solids Struct.* **41** 1357–75

[10] Mitchell J A and Reddy J N 1995 A refined hybrid plate theory for composite laminates with piezoelectric laminae *Int. J. Solids Struct.* **32** 2345–67

[11] Yu W, Hodges D H and Volovoi V V 2002 Asymptotic construction of Reissner-like models for composite plates with accurate strain recovery *Int. J. Solids Struct.* **39** 5185–203

[12] Yu W, Hodges D H and Volovoi V V 2002 Asymptotic generalization of Reissner–Mindlin theory: accurate three-dimensional recovery for composite shells *Comput. Methods Appl. Mech. Eng.* **191** 5087–109

[13] Yu W and Hodges D H 2004 An asymptotic approach for thermoelastic analysis of laminated composite plates *J. Eng. Mech.* **130** 531–40

[14] Yu W and Hodges D H 2004 A simple thermopiezoelastic model for composite plates with accurate stress recovery *Smart Mater. Struct.* **13** 926–38

[15] Berdichevsky V L 1979 Variational-asymptotic method of constructing a theory of shells *Prikladnaya Matematika i Mekhanika* **43** 664–87

[16] Reissner E 1974 Linear and nonlinear theory of shells *Thin Shell Structures* ed Y C Fung and E E Sechler (Englewood Cliffs, NJ: Prentice-Hall) pp 29–44

[17] Danielson D A and Hodges D H 1987 Nonlinear beam kinematics by decomposition of the rotation tensor *J. Appl. Mech.* **54** 258–62

[18] Hodges D H, Atılgan A R and Danielson D A 1993 A geometrically nonlinear theory of elastic plates *J. Appl. Mech.* **60** 109–16

[19] Yu W and Hodges D H 2004 A geometrically nonlinear shear deformation theory for composite shells *J. Appl. Mech.* **71** 1–9

[20] Sutyrin V G 1997 Derivation of plate theory accounting asymptotically correct shear deformation *J. Appl. Mech.* **64** 905–15

[21] Dube G P, Kapuria S and Dumir P C 1996 Exact piezothermoelastic solution of simply-supported orthotropic cylindrical panel in cylindrical bending *Arch. Appl. Mech.* **66** 537–54

[22] Bauchau O A, Bottasso C L and Nikishkov Y G 2001 Modeling rotorcraft dynamics with finite element multibody procedures *Math. Comput. Modelling* **33** 1113–37